




Time-reversal invariant topological gapped phases in bilayer Dirac materialsGuan-Hao Feng , Hong-Hao Zhang ,* and Zhongbo Yan [†]*Guangdong Provincial Key Laboratory of Magnetoelectric Physics and Devices, School of Physics, Sun Yat-sen University, Guangzhou 510275, China*

(Received 21 May 2022; revised 17 August 2022; accepted 18 August 2022; published 22 August 2022)

We show that a plethora of topological insulating phases can appear in bilayer Dirac materials, including first-order topological insulators, topological mirror insulators, and second-order topological insulators. By considering doping and short-range attractive interactions, we show at a mean-field level that intrinsic odd-parity superconductivity can arise in such systems. Depending on the number and positions of Fermi surfaces in the normal state, we find that the resulting odd-parity superconductivity can lead to diverse time-reversal invariant topological superconducting phases, including topological superconductors and topological mirror superconductors. Our findings suggest that bilayer Dirac materials could be an excellent platform for investigating topological phases.

DOI: [10.1103/PhysRevB.106.064509](https://doi.org/10.1103/PhysRevB.106.064509)**I. INTRODUCTION**

Topological insulators and superconductors have attracted great attention in the past two decades [1,2]. The great interest in these two classes of materials lies in their host of novel gapless boundary states enforced by bulk-boundary correspondence which hold great promise for revolutionizing future technology and science. Originally, topological insulators and superconductors were classified into ten symmetry classes according to three internal symmetries [3–5], namely, time-reversal symmetry, particle-hole symmetry, and chiral (sublattice) symmetry. Because of the protection from the internal symmetry, the gapless boundary states are not sensitive to the shape or the orientation of the boundary and robust against imperfections on the boundary. Later, it was found that gapless boundary states can also be protected by various crystalline symmetries [6], accompanied by the birth of the concept termed topological crystalline insulators and superconductors [7]. Owing to the richness of crystalline symmetry, this greatly enriches the topological phases and brings new features to the gapless boundary states [8–16]. For instance, if the crystalline symmetry is essential for the definition of a nontrivial bulk topology, robust gapless boundary states will only exist on the boundaries respecting the exact crystalline symmetry. Remarkably, recently it was recognized that such an orientation dependence admits the emergence of gapless states with codimension $d_c \geq 2$ on the boundary [17–22]. Topological insulators and superconductors displaying such unconventional bulk-boundary correspondence are categorized as higher-order topological insulators and superconductors [23–25] to distinguish them from conventional (also dubbed first-order) topological insulators and superconductors.

Topological superconductors in fact have a close connection to topological insulators not only in the mathematical description but also in their realizations. After the discovery of topological insulators in experiments, the potential of achieving topological superconductivity and concomitant Majorana zero modes in superconducting doped topological insulators has attracted wide interest [26]. The first material realization of the superconducting doped topological insulator is the three-dimensional topological insulator Bi_2Se_3 with copper intercalation [27–29]. On the theoretical side, Fu and Berg theoretically analyzed the potential superconducting pairings in superconducting doped insulators based on a two-orbital model and the assumption of short-range attractive interactions, and they found that an odd-parity spin-triplet pairing, which can lead to the realization of time-reversal invariant topological superconductivity, is favored by the strong spin-orbit coupling [30]. On the experimental side, soon after the observation of superconductivity in $\text{Cu}_x\text{Bi}_2\text{Se}_3$, the observation of a zero-bias conductance peak in point-contact experiments in this material had generated much excitement as it was interpreted as a strong signature for the emergence of unconventional superconductivity [31]. Later, superconductivity and similar zero-bias peaks had also been observed in doped SnTe [32], a topological crystalline insulator [33–39]. More recently, a remarkable experimental progress along this route was the observation of topological band structure and signatures for vortex Majorana zero modes in a series of iron-based superconductors [40–44]. Despite the fact that the pairings in iron-based superconductors are generally believed to be of even parity which cannot result in first-order time-reversal invariant topological superconductivity with the constraint of inversion symmetry [45], it was predicted in theory that time-reversal invariant higher-order topological superconductivity could arise in this class of materials [45–49].

Despite this remarkable progress in three-dimensional superconducting doped topological insulators, the unequivocal

* zhh98@mail.sysu.edu.cn

[†] yanzhb5@mail.sysu.edu.cn

detection of topological superconductivity, not to mention topological phase transitions between distinct topological superconducting phases, has been hindered due to the lack of efficient methods to tune the parameters of a given system in a clean and controllable way. In particular, the carrier density in bulk materials, a key quantity to achieve superconductivity and control the superconducting pairing and bulk topology, are generally tuned by doping other elements or a partial substitution of the constituent elements [50]. Such a procedure, however, will generally inevitably induce inhomogeneity to the sample, which may either reduce the superconducting transition temperature or obscure the detection of topological boundary states by introducing other energy-close bound states. Compared to three-dimensional systems, two-dimensional systems show great advantage in tunability, and accordingly have rapidly grown as one of the most active fields after the first experimental realization of monolayer graphene [51]. Remarkably, the carrier density in two-dimensional systems can be controlled by gate-voltage methods which are clean and reversible [52]. Moreover, for van der Waals materials, the number of layers is easy to control and thus can be applied as a new degree of freedom to realize novel physics. Given these advantages, superconducting two-dimensional topological materials appears to be a better platform to implement and investigate various kinds of topological superconducting phases [53].

How to realize topological superconductivity in two-dimensional materials has also been extensively studied over the past decade [54–57]. Focusing on time-reversal invariant systems, it has been theoretically recognized that the realization of time-reversal invariant first-order topological superconductors requires the superconducting pairing to be unconventional, such as being odd parity or momentum dependent [48,58–64]. For time-reversal invariant higher-order topological superconductors, it has been revealed that a general approach for their realization is to consider heterostructures composed of first-order topological insulators and unconventional superconductors [65–67]. Compared to first-order and higher-order topological superconductors, we notice that realistic proposals for time-reversal invariant topological crystalline superconductors in simple lattices remain lacking. In Refs. [68,69] the authors proposed that multilayer superconductors CeCoIn_5 can favor topological mirror superconducting phases when the ground state takes a pairing-density-wave order. However, the stabilization of such an order is shown to require a magnetic field, which breaks time-reversal symmetry explicitly. Topological crystalline superconductors stabilized by magnetic field or nonsymmorphic symmetry have also been suggested in UPt_3 [70,71], Sr_2RuO_4 [72], CeRh_2As_2 [73], UCoGe [74], etc., but remain unconfirmed in experiments. Furthermore, we notice that many studies in the literatures focus on a particular type of topological superconductors. It will be of great interest if a single system can host various types of time-reversal invariant topological superconductivity and the transitions between them can be simply tuned by varying the doping level. In this work we show that bilayer Dirac materials could be such systems.

Over the past decade, bilayer Dirac materials with threefold or sixfold rotation symmetry have been actively studied

and many novel physics have been found [75–78]. In the past few years, exotic superconductivity has been observed in a series of transition metal dichalcogenides with massive Dirac band structure, such as MoS_2 [79–81], NbSe_2 [82], WTe_2 [83], etc. More recently, the observation of correlated insulating phases and superconductivity in twisted bilayer graphene has generated further excitement [84–88]. With this experimental progress, potential topological superconducting phases in bilayer Dirac materials have also been actively investigated in theory [89–95], but most of these studies focused on time-reversal symmetry breaking topological superconductivity.

Compared to the bilayer Dirac systems with threefold or sixfold rotation symmetry, we notice that bilayer Dirac systems with simple square lattice structure and fourfold rotation symmetry have been much less explored. In this work we consider bilayer Dirac systems with the D_{4h} crystal symmetry which can be implemented by either a stacking of two monolayer spin-orbit-coupled insulators [96] or a reduction of a three-dimensional spin-orbit-coupled insulator/Dirac semimetal to the bilayer limit [48]. At the free-particle level, we find that the normal state can support a plethora of topological insulating phases. Depending on the band-inversion parameter and interlayer coupling, the normal-state band structure can exhibit all three types of time-reversal invariant topological insulating phases, namely, the first-order topological insulator, the topological crystalline (mirror) insulator, and the higher-order topological insulator. Considering short-range attractive interactions, we find that, similar to previous studies on superconducting doped topological insulators, odd-parity superconductivity can be favored under appropriate conditions due to spin-orbit coupling [30]. Depending on the doping level, we find that the odd-parity superconductivity can result in a diversity of time-reversal invariant topological superconducting phases protected by the internal symmetry and mirror symmetry.

The structure of the paper is as follows. In Sec. II we discuss the topological properties of the normal state, showing that a plethora of time-reversal invariant topological insulating phases can emerge by varying the model parameters. In Sec. III we show that, after considering finite doping, the system can favor odd-parity superconductivity under appropriate conditions. In Sec. IV we show that the odd-parity superconductivity can result in time-reversal invariant topological superconductors protected by internal and mirror symmetries. Discussion and conclusion are presented in Sec. V.

II. TOPOLOGICAL PROPERTIES OF THE NORMAL STATE

Adopting a minimal tight-binding model approach, we consider the following Hamiltonian:

$$\begin{aligned} \mathcal{H}_0(\mathbf{k}) = & (m - t \cos k_x - t \cos k_y) \Sigma_{300} + \lambda \sin k_x \Sigma_{130} \\ & - \lambda \sin k_y \Sigma_{200} + \eta_1 (\cos k_x - \cos k_y) \Sigma_{112} \\ & + \eta_2 \sin k_x \sin k_y \Sigma_{122} - t_z \Sigma_{301}, \end{aligned} \quad (1)$$

where $\Sigma_{ijk} = \sigma_i \otimes s_j \otimes \rho_k$ with σ_i , s_j , and ρ_k being the Pauli matrices (identity matrices for subscript “0”) in orbital, spin, and layer subspaces, respectively. For notational simplicity,

the lattice constants are set to unity throughout the paper. Furthermore, we have assumed that the Hamiltonian has a nearly perfect particle-hole symmetry, so terms of the form $\epsilon(\mathbf{k})\Sigma_{000}$ describing particle-hole asymmetry [$\epsilon(\mathbf{k})$ denotes a real and even function of momentum] are neglected for simplicity. When $0 < |m| < 2t$, the first three terms describe two decoupled monolayer topological insulators [97]. On the contrary, when $|m| > 2t$, the first three terms describe two decoupled monolayer spin-orbit-coupled trivial insulators. The last three terms describe layer couplings respecting time-reversal symmetry [$\mathcal{T}\mathcal{H}_0(\mathbf{k})\mathcal{T}^{-1} = \mathcal{H}_0(-\mathbf{k})$ with $\mathcal{T} = i\Sigma_{020}\mathcal{K}$ and \mathcal{K} the complex conjugate operator], inversion symmetry [$\mathcal{I}\mathcal{H}_0(\mathbf{k})\mathcal{I}^{-1} = \mathcal{H}_0(-\mathbf{k})$ with $\mathcal{I} = \Sigma_{103}$], C_{4z} rotation symmetry [$C_{4z}\mathcal{H}_0(k_x, k_y)C_{4z}^{-1} = \mathcal{H}_0(k_y, -k_x)$ with $C_{4z} = (\Sigma_{300} - i\Sigma_{030})/\sqrt{2}$], and mirror symmetry about the middle plane of the two layers [$\mathcal{M}_z\mathcal{H}_0(\mathbf{k})\mathcal{M}_z^{-1} = \mathcal{H}_0(\mathbf{k})$ with $\mathcal{M}_z = i\Sigma_{031}$]. The whole Hamiltonian belongs to the D_{4h} symmetry group.

Based on the symmetry analysis and the tenfold-way classification, the Hamiltonian falls into the class AII and thus follows the Z_2 classification if one only considers protection from the internal time-reversal symmetry [3–5]. Accordingly, one may naively expect that the stacking of two identical monolayer insulators should result in a trivial insulator since “2” is topologically equivalent to “0,” the trivial case. From the edge-state point of view, this is equivalent to saying that, if the bilayer system is a stacking of two monolayer topological insulators, two pairs of helical edge states can hybridize with each other and be gapped out. However, this scenario is valid only within the weak-interlayer-coupling regime and when there is no other symmetry protection. As we will show in the following, because of the additional protection from the mirror symmetry \mathcal{M}_z , multiple pairs of helical edge states can also be stable. Moreover, depending on the band-inversion parameter m and the interlayer-coupling parameters t_z and η_1 , we find that the bilayer system can realize time-reversal invariant first-order topological insulating phases with helical edge states as well as second-order topological insulating phases with localized bound states at the system’s corners. It is worth emphasizing that strong-enough interlayer coupling can drive the bilayer system to be topological even when the monolayer counterpart is trivial.

Let us first focus on the Z_2 invariant related to time-reversal symmetry. Because the Hamiltonian also has inversion symmetry, it is known that the Z_2 invariant is determined by the Fu-Kane formula [98]

$$(-1)^\nu = \prod_{n \in \text{occ}} \prod_i \xi_{2n}(\Gamma_i), \quad (2)$$

where $\xi_{2n}(\Gamma_i) = \langle 2n, \Gamma_i | \mathcal{I} | 2n, \Gamma_i \rangle$ refers to the parity of the n th occupied Kramers bands at the time-reversal invariant momentum Γ_i . Before explicitly calculating ν , let us first discuss the topological characterization enriched by the mirror symmetry. For the bilayer system, since $[\mathcal{M}_z, \mathcal{H}_0(\mathbf{k})] = 0$ for an arbitrary \mathbf{k} , it means that the Hamiltonian can be decoupled into two independent blocks according to the two eigenvalues of the mirror operator $\mathcal{M}_z = i\Sigma_{031}$, i.e., $\mathcal{H}_0(\mathbf{k}) = \mathcal{H}_0^{+i}(\mathbf{k}) \oplus \mathcal{H}_0^{-i}(\mathbf{k})$. In the diagonal basis of \mathcal{M}_z , one finds

$$\begin{aligned} \mathcal{H}_0^{\pm i}(\mathbf{k}) = & (m - t \cos k_x - t \cos k_y)\Sigma_{30} + \lambda \sin k_x \Sigma_{13} \\ & - \lambda \sin k_y \Sigma_{20} \pm \eta_1 (\cos k_x - \cos k_y)\Sigma_{12} \\ & \mp \eta_2 \sin k_x \sin k_y \Sigma_{11} \mp t_z \Sigma_{33}. \end{aligned} \quad (3)$$

While the total Hamiltonian $\mathcal{H}_0(\mathbf{k})$ has time-reversal symmetry, each mirror block does not preserve it, and one can easily find that $\mathcal{H}_0^{\pm i}(\mathbf{k})$ belong to the A class, indicating that their band topological properties are respectively characterized by the first-class Chern number [3–5]. Labeling the Chern number characterizing $\mathcal{H}_0^{\pm i}(\mathbf{k})$ as $C_{\pm i}$, the time-reversal symmetry of the total Hamiltonian forces the total Chern number $C_T = C_{+i} + C_{-i}$ to vanish, thus the relation $C_{+i} = -C_{-i}$ is always held as long as the time-reversal symmetry is preserved. The relation $C_{+i} = -C_{-i}$ indicates that $\mathcal{H}_0^{+i}(\mathbf{k})$ and $\mathcal{H}_0^{-i}(\mathbf{k})$ carry an equal number of chiral edge states but with opposite chiralities on the same edge. Following the standard definition [99], the mirror Chern number is given by

$$C_M = (C_{+i} - C_{-i})/2. \quad (4)$$

A nonzero C_M dictates the existence of C_M pairs of gapless helical states on the open edges. As C_M can take an arbitrary integer value, this indicates that the Z_2 classification is extended to a Z classification due to the additional protection from the mirror symmetry \mathcal{M}_z . It is worth noting that the Z_2 -valued topological invariant ν and the integer-valued C_M are not completely independent. One can easily infer from the protected helical edge states that the even-odd parities of ν and C_M are equal to each other, i.e.,

$$(-1)^\nu = (-1)^{C_M}. \quad (5)$$

When C_M is odd, the topological insulator can be viewed as a dual topological insulator due to the double topological characterizations [100–103].

The phase diagram of $\mathcal{H}_0(\mathbf{k})$ can be mapped out by determining the phase boundaries and the topological invariants in parameter spaces away from the phase boundaries. Because the change of first-order topology is associated with the closure of bulk gap which turns out to be possible only at the four time-reversal invariant momenta, one can find that the phase boundaries are determined by the following three equations:

$$\begin{aligned} |t_z| &= |m - 2t|, \\ |t_z| &= |m + 2t|, \\ |t_z| &= \sqrt{m^2 + 4\eta_1^2}. \end{aligned} \quad (6)$$

For a given fixed η_1/t , we obtain the phase diagram by numerically calculating C_M , as shown in Fig. 1(a). For the considered tight-binding model, we find that C_M ranges from -2 to 2 . In other words, the number of pairs of gapless helical edge states is up to 2 . According to the discussions given above, $C_M = \pm 1$ corresponds to a dual topological insulator with a pair of gapless helical states protected by both time-reversal symmetry and mirror symmetry, as shown in Fig. 1(b). On the other hand, $C_M = \pm 2$ merely corresponds to a topological mirror insulator with two pairs of gapless helical edge states protected by the mirror symmetry only, as shown in Fig. 1(c). When $C_M = 0$, remarkably, we find that the resulting insulating phases can be further delicately classified as truly topologically trivial insulators and second-order

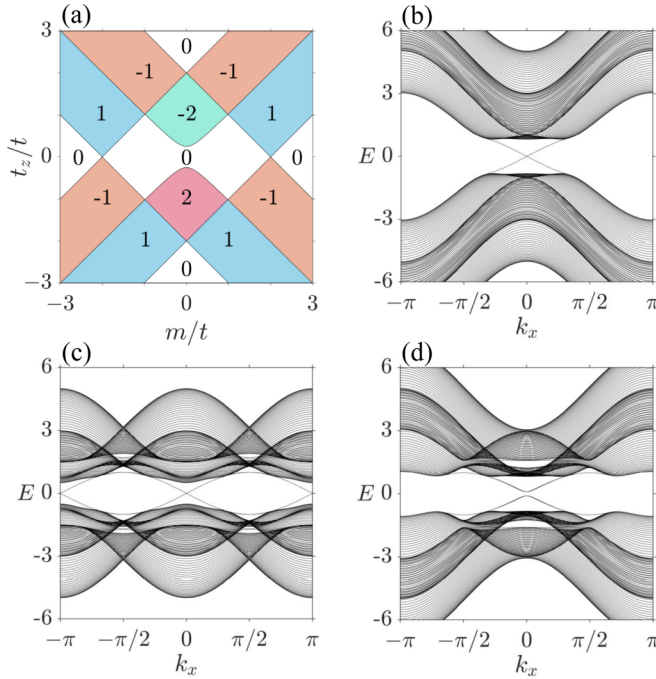


FIG. 1. (a) A representative topological phase diagram $\eta_1/t = 0.125$. The values inside are the corresponding mirror Chern numbers. (b)–(d) The energy spectra of the bilayer system with open boundary conditions in the y direction and periodic boundary conditions in the x direction. In (b)–(d), m is equal to 4, 0, and 2, respectively, and other parameters are chosen as $\{t, t_z, \lambda, \eta_1, \eta_2\} = \{2, 1, 1, 0.25, 0.25\}$. The mirror Chern numbers for (b)–(d) are $C_M = 1, 2$, and 0, respectively.

topological insulators. For the latter, while there are no gapless helical edge states under the cylindrical boundary condition (one direction is open and the other is periodic) [see Fig. 1(d)], midgap bound states with codimension $d_c = 2$ are found to emerge at the system's corners when both directions of the system are set to be open, as shown in Fig. 2.

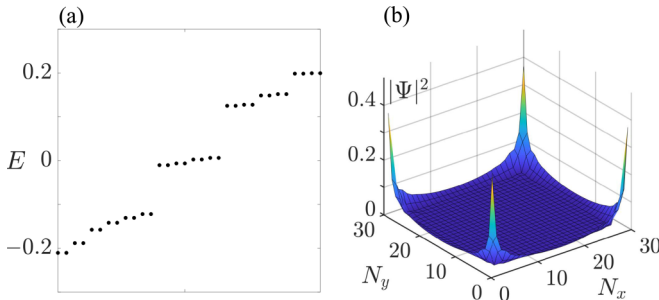


FIG. 2. Second-order topological insulator with corner bound states. (a) Energy eigenvalues near zero energy for a system with open boundary conditions in both x and y directions. The lattice size is $N_x = N_y = 30$. (b) The probability density profiles of the eight eigenstates with eigenenergies closest to zero energy, i.e., $|\Psi(i, j)|^2 = \sum_{\alpha=1}^8 |\Psi_{\alpha}(i, j)|^2$. Chosen parameters are $\{m, t, t_z, \lambda, \eta_1, \eta_2\} = \{2, 2, 1, 1, 0.25, 0.25\}$, corresponding to $C_M = 0$.

Here the possibility of the emergence of a second-order topological insulating phase can be intuitively understood via a perturbation-theory picture [65]. The procedures are as follows. In the first place, one decomposes the Hamiltonian into two parts, $\mathcal{H}_0(\mathbf{k}) = \mathcal{H}_1(\mathbf{k}) + \mathcal{H}_2(\mathbf{k})$, where

$$\mathcal{H}_1(\mathbf{k}) = (m - t \cos k_x - t \cos k_y) \Sigma_{300} + \lambda \sin k_x \Sigma_{130} - \lambda \sin k_y \Sigma_{200} - t_z \Sigma_{301},$$

$$\mathcal{H}_2(\mathbf{k}) = \eta_1 (\cos k_x - \cos k_y) \Sigma_{112} + \eta_2 \sin k_x \sin k_y \Sigma_{122}. \quad (7)$$

Second, treat $\mathcal{H}_2(\mathbf{k})$ as perturbations. Compared to $\mathcal{H}_0(\mathbf{k})$, $\mathcal{H}_1(\mathbf{k})$ has higher symmetry as a consequence of removing the terms in $\mathcal{H}_2(\mathbf{k})$. It is easy to find that $\mathcal{H}_1(\mathbf{k})$ can be expressed as the direct sum of four two-by-two Hamiltonians according to the eigenvalues of s_3 and ρ_1 , i.e., $\mathcal{H}_1 = \mathcal{H}_{1,1} \oplus \mathcal{H}_{1,-1} \oplus \mathcal{H}_{-1,1} \oplus \mathcal{H}_{-1,-1}$. When $\mathcal{H}_{\pm 1, \pm 1}(\mathbf{k})$ all harbor a chiral edge state crossing the same time-reversal invariant momentum, they will form two pairs of helical edge states even though $C_M = 0$. The absence of hybridization among the four branches of chiral edge states (two counterclockwise, the other two clockwise) is because they take different quantum numbers as s_3 and ρ_1 are conserved in $\mathcal{H}_1(\mathbf{k})$. After turning on $\mathcal{H}_2(\mathbf{k})$, however, both s_3 and ρ_1 are no longer conserved, then the hybridization is allowed and a finite energy gap will be opened on the edges. Interestingly, by projecting $\mathcal{H}_2(\mathbf{k})$ onto the Hilbert space spanned by the eigenstates of the two pairs of helical edge states, one can find that the Dirac mass reflecting the hybridization induced by the η_1 term will have opposite signs on the x -normal edges and the y -normal edges, resulting in the formation of domain walls with bound states at each corner of a square sample with open boundary conditions along both x and y directions [65]. It is worth noting that if $\eta_2 = 0$ and the system size is sufficiently large, the corner modes will be pinned to zero energy due to the emergence of chiral symmetry.

We end this part by stressing that the above results indicate that time-reversal invariant first-order (or dual) topological insulators, topological mirror insulators, as well as second-order topological insulators can all be achieved in such bilayer Dirac systems.

III. SUPERCONDUCTIVITY INDUCED BY ON-SITE ATTRACTIVE INTERACTIONS

The bilayer system is expected to become superconducting if it is doped to be metallic and the electrons feel effective attractive interactions. In the following we focus on on-site attractive interactions and investigate what kind of pairing order parameters will be favored in this system. The interactions are assumed to be purely on-site and take the form [30]

$$H_{\text{int}} = -U \sum_{i,\rho} (n_{i,1,\rho}^2 + n_{i,2,\rho}^2) - 2V \sum_{i,\rho} n_{i,1,\rho} n_{i,2,\rho}, \quad (8)$$

where U (V) characterizes the strength of the intraorbital (interorbital) interaction, and $n_{i,\sigma,\rho} = \sum_{s=\uparrow,\downarrow} c_{i,\sigma,s,\rho}^\dagger c_{i,\sigma,s,\rho}$ refers to the electron density operator for a given σ orbital at site i and layer ρ . U and V are assumed to be positive in this work.

Within the mean-field framework, the on-site attractive interactions will only result in momentum-independent

TABLE I. Classification of the pairings according to the irreducible representations of the crystal point group D_{4h} .

Representation	Matrix form	Explicit form
$A_{1g}: \Delta_1$	$\Sigma_{000}, \Sigma_{300}$	$c_{1\uparrow}c_{1\downarrow} + c_{2\uparrow}c_{2\downarrow}, c_{1\uparrow}c_{1\downarrow} - c_{2\uparrow}c_{2\downarrow}$
$A_{1u}: \Delta_2$	Σ_{220}	$c_{1\uparrow}c_{2\uparrow} + c_{1\downarrow}c_{2\downarrow}$
$A_{2u}: \Delta_3$	Σ_{210}	$i(c_{1\uparrow}c_{2\uparrow} - c_{1\downarrow}c_{2\downarrow})$
$E_u: \Delta_4$	$\Sigma_{230}, \Sigma_{100}$	$i(c_{1\uparrow}c_{2\downarrow} + c_{1\downarrow}c_{2\uparrow}), c_{1\uparrow}c_{2\downarrow} - c_{1\downarrow}c_{2\uparrow}$

pairings. After entering the superconducting phase, the system is described by a Bogoliubov–de Gennes (BdG) Hamiltonian. In the Nambu basis $\Psi_k^\dagger = [\psi_k^\dagger, (i\Sigma_{020}\psi_{-k})^T]$, the Hamiltonian has the form $H = \frac{1}{2} \sum_k \Psi_k^\dagger \mathcal{H}_{\text{BdG}}(\mathbf{k}) \Psi_k$ with

$$\begin{aligned} \psi_k^\dagger &= (\psi_{k,1}^\dagger, \psi_{k,2}^\dagger), \\ \psi_{k,\alpha}^\dagger &= (c_{k;\alpha,\uparrow,t}^\dagger, c_{k;\alpha,\uparrow,b}^\dagger, c_{k;\alpha,\downarrow,t}^\dagger, c_{k;\alpha,\downarrow,b}^\dagger), \\ \mathcal{H}_{\text{BdG}}(\mathbf{k}) &= \tau_z \otimes [\mathcal{H}_0(\mathbf{k}) - \mu \Sigma_{000}] + \tau_x \otimes \Delta(\mathbf{k}), \end{aligned} \quad (9)$$

where $\Delta(\mathbf{k})$ represents the pairing matrix which is 8×8 here, μ is the chemical potential, and τ_i are the Pauli matrices in particle-hole space. The subscripts (1,2), (\uparrow, \downarrow), and (t, b) refer to the orbital, spin, and layer degrees of freedom, respectively. For the pairings, because of the anticommutation relation between fermionic operators, here only six possible pairings are allowed. We list them in Table I according to the representation of the underlying crystal point group D_{4h} . Among them, the pairings belonging to the irreducible representation A_{1g} are of even parity, and the pairings belonging to A_{1u}, A_{2u} , and E_u are all of odd parity.

To determine which pairing will be favored in energy, one can first make a rough estimation by taking the mean-field pairing back into the BdG Hamiltonian and checking whether the considered pairing results in a gapless or fully gapped energy spectrum. Simple analysis reveals that the pairing in the two-dimensional representation E_u will lead to nodal superconductors, while the pairings in the one-dimensional representations A_{1g}, A_{1u} , and A_{2u} will lead to fully gapped superconductors. It is known that, for superconducting instability under the same condition, a fully gapped superconductor is in general favored in energy. Therefore, based on this estimation, the pairings in the three one-dimensional representations should win over the ones in the two-dimensional representation.

To determine the pairing phase diagram on a firmer ground, we solve the linearized gap equations for the superconducting transition temperature (T_c) in each pairing channel [30,60]. The linearized gap equations are of the form (see details in Appendices A–F)

$$\begin{aligned} \det \left[\begin{pmatrix} U \chi_{1,11}(T_c) & U \chi_{1,12}(T_c) \\ U \chi_{1,21}(T_c) & U \chi_{1,22}(T_c) \end{pmatrix} - I_{2 \times 2} \right] &= 0, \\ V \chi_2(T_c) = V \chi_3(T_c) = 1, \quad V \chi_4(T_c) &= 1. \end{aligned} \quad (10)$$

Here χ_i denote finite-temperature superconducting susceptibilities in different pairing channels. Without loss of generality, by assuming that the normal-state band minima are located at the time-reversal invariant momentum $\mathbf{\Gamma} = (0, 0)$, we find that in the limit of $\eta_1 = \eta_2 = 0$ their explicit forms

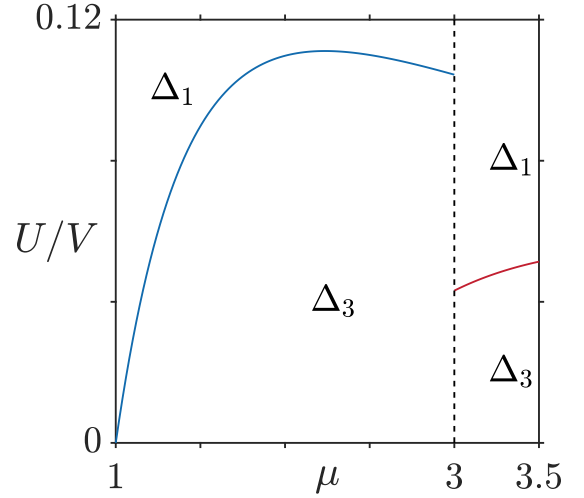


FIG. 3. A representative pairing phase diagram. The parameters for the normal-state Hamiltonian are chosen as $\{m, t, t_z, \lambda, \eta_1, \eta_2\} = \{6, 2, 1, 1, 0, 0\}$. The discontinuous jump at $\mu = 3$ is because the Fermi surface undergoes a Lifshitz transition there.

are given by (see details in Appendices B–E)

$$\begin{aligned} \chi_{1,11} &= (D_1 + D_2)\chi_0, \\ \chi_{1,12} &= \chi_{1,21} = (D_1\Lambda_1 + D_2\Lambda_2)\chi_0, \\ \chi_{1,22} &= (D_1\Lambda_1^2 + D_2\Lambda_2^2)\chi_0, \\ \chi_2 &= \chi_3 = [D_1(1 - \Lambda_1^2) + D_2(1 - \Lambda_2^2)]\chi_0, \\ \chi_4 &< \chi_2 = \chi_3, \end{aligned} \quad (11)$$

where $\Lambda_1 \equiv (M_1 - t_z)/\mu$ and $\Lambda_2 \equiv (M_2 + t_z)/\mu$, and $\chi_0 = \int d\xi \frac{1}{\xi} \tanh \frac{\beta\xi}{2}$ with $\beta = 1/(k_B T)$ is the standard superconducting susceptibility normalized by the density of states at Fermi energy. The quantities D_1 and D_2 refer to the density of states at Fermi energy contributed by the first and second pair of Kramers bands, respectively. The quantities M_1 and M_2 refer to the value $M(\mathbf{k}) = m - t \cos k_x - t \cos k_y$ on the two Fermi surfaces and are approximated as constants. If the Fermi level only crosses the lowest pair of Kramers bands, there is only one Fermi surface, then $D_2 = 0$ and only D_1 is involved in the superconducting susceptibilities (see details in Appendix F). It is worth noting that $\chi_i(T)$ are monotonically decreasing functions of T . The fact that χ_4 is always smaller than $\chi_{2,3}$ indicates that Δ_4 always has a lower T_c than $\Delta_{2,3}$, so it will not appear in the pairing phase diagram. Furthermore, it is worth noting that while χ_2 and χ_3 are degenerate in the limit of $\eta_1 = \eta_2 = 0$, we find numerically that Δ_3 will result in a somewhat lower ground-state energy compared to Δ_2 if η_2 is nonzero. Therefore, we will only show Δ_3 in the pairing phase diagram.

Based on Eqs. (10) and (11), the pairing phase diagram can be mapped out. In Fig. 3 we present one concrete case for illustration. According to the pairing phase diagram, it is readily found that odd-parity pairing is favored in the small U/V limit, which is physically consistent with the fact that only V leads to interorbital pairings.

IV. TOPOLOGICAL PROPERTIES OF THE BILAYER SYSTEM WITH ODD-PARITY SUPERCONDUCTIVITY

While the pairing phase diagram contains both even-parity and odd-parity pairings, the even-parity pairing will only result in topologically trivial phases as the system has both time-reversal symmetry and inversion symmetry [104]. Therefore, below we focus on Δ_3 and study the potential topological superconductivity. Write down the BdG Hamiltonian explicitly,

$$\begin{aligned} \mathcal{H}_{\text{BdG}}(\mathbf{k}) = & (m - t \cos k_x - t \cos k_y) \Sigma_{3300} + \lambda \sin k_x \Sigma_{3130} \\ & - \lambda \sin k_y \Sigma_{3200} + \eta_1 (\cos k_x - \cos k_y) \Sigma_{3112} \\ & + \eta_2 \sin k_x \sin k_y \Sigma_{3122} - t_z \Sigma_{3301} - \mu \Sigma_{3000} \\ & + \Delta_3 \Sigma_{1210}, \end{aligned} \quad (12)$$

where $\Sigma_{ijkl} = \tau_i \otimes \sigma_j \otimes s_k \otimes \rho_l$. Within the BdG framework, it is known that the Hamiltonian has an intrinsic particle-hole symmetry (the corresponding symmetry operator is $\Xi = \Sigma_{2020} \mathcal{K}$). Accordingly, the time-reversal invariant BdG Hamiltonian belongs to the DIII class which follows a Z_2 classification in two dimensions [3–5]. On the other hand, since the pairing respects all crystal symmetries, the BdG Hamiltonian can also be decomposed into two independent blocks according to the two eigenvalues of the mirror symmetry operator. It is worth noting that the form of the mirror symmetry operator now becomes $\mathcal{M}_z = i \Sigma_{3031}$. In the diagonal basis of \mathcal{M}_z , one finds $\mathcal{H}_{\text{BdG}}(\mathbf{k}) = \mathcal{H}_{\text{BdG}}^{+i}(\mathbf{k}) \oplus \mathcal{H}_{\text{BdG}}^{-i}(\mathbf{k})$, where

$$\begin{aligned} \mathcal{H}_{\text{BdG}}^{\pm i}(\mathbf{k}) = & (m - t \cos k_x - t \cos k_y) \Sigma_{330} + \lambda \sin k_x \Sigma_{313} \\ & - \lambda \sin k_y \Sigma_{320} \pm \eta_1 (\cos k_x - \cos k_y) \Sigma_{012} \\ & \pm \eta_2 \sin k_x \sin k_y \Sigma_{011} \mp t_z \Sigma_{033} - \mu \Sigma_{300} \\ & + \Delta_3 \Sigma_{121}. \end{aligned} \quad (13)$$

It is easy to find that the time-reversal symmetry is broken while the particle-hole symmetry (the symmetry operator becomes $\Xi = \Sigma_{202} \mathcal{K}$) is preserved in each mirror sector. According to the tenfold way classification, each mirror sector belongs to the D class and follows a Z classification in two dimensions [3–5]. As the topological invariant characterizing the D class is also the first-class Chern number, the topological analysis for the BdG Hamiltonian can be done just like the normal state. Because the BdG Hamiltonian has inversion symmetry and the pairing is odd parity, in the weak-coupling limit the Z_2 invariant characterizing the full BdG Hamiltonian is simply determined by the parity of the number of time-reversal invariant momentum enclosed by the Fermi surface [30,105],

$$(-1)^{\nu_s} = \prod_i (-1)^{N(\Gamma_i)}, \quad (14)$$

where $N(\Gamma_i)$ refers to the number of unoccupied bands at Γ_i in the normal state. When the Fermi surface of the normal state encloses an odd (even) number of time-reversal invariant momenta, $\nu_s = 1(0)$, corresponding to a time-reversal invariant topological (Z_2 -trivial) superconductor with an odd (even, including zero) number of pairs of helical Majorana edge states. Taking into account the mirror symmetry \mathcal{M}_z , a mirror

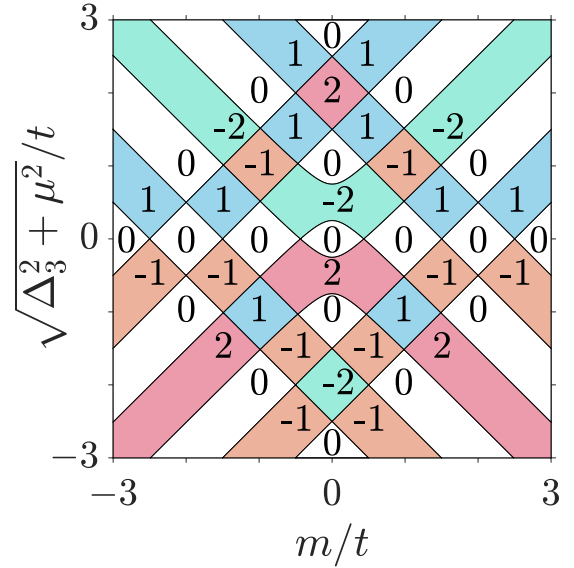


FIG. 4. A representative phase diagram of the odd-parity superconductor. $\eta_1/t = 0.125$ and $t_z/t = 0.5$ are fixed. We have labeled the values of the mirror Chern number inside each parameter region.

Chern number can be similarly defined as

$$C_{M,s} = (C_s^{+i} - C_s^{-i})/2. \quad (15)$$

When $C_{M,s}$ is nonzero, the superconductor is also a topological mirror superconductor with $C_{M,s}$ pairs of helical Majorana edge states [106]. Apparently these two topological invariants also have the relation

$$(-1)^{\nu_s} = (-1)^{C_{M,s}}. \quad (16)$$

This relation suggests that the phase diagram can be unitedly determined by the mirror Chern number. The phase boundaries can also be simply determined by checking the condition for the closure of bulk energy gap. Simple analysis reveals that the bulk energy gap can only close at time-reversal invariant momenta and the phase boundaries are determined by the following equations:

$$\begin{aligned} \sqrt{\Delta_3^2 + \mu^2} &= |\pm(m - 2t) \pm t_z|, \\ \sqrt{\Delta_3^2 + \mu^2} &= |\pm(m + 2t) \pm t_z|, \\ \sqrt{\Delta_3^2 + \mu^2} &= \left| \pm \sqrt{m^2 + 4\eta_1^2} \pm t_z \right|. \end{aligned} \quad (17)$$

By numerically determining the mirror Chern number, we provide a representative phase diagram in Fig. 4. According to the phase diagram, the mirror Chern number can take values $\{-2, -1, 0, 1, 2\}$, suggesting that the number of pairs of robust helical Majorana edge states is up to two in this model. Similar to the normal state, the bulk-boundary correspondence indicates that when $C_{M,s} = \pm 1$, the superconductor carries a pair of helical Majorana edge states, and corresponds to a first-order internal-symmetry-protected topological superconductor as well as a topological mirror superconductor. When $C_{M,s} = \pm 2$, the superconductor carries two pairs of helical Majorana edge states and is purely a topological mirror superconductor. Remarkably, as we will show below, two pairs of

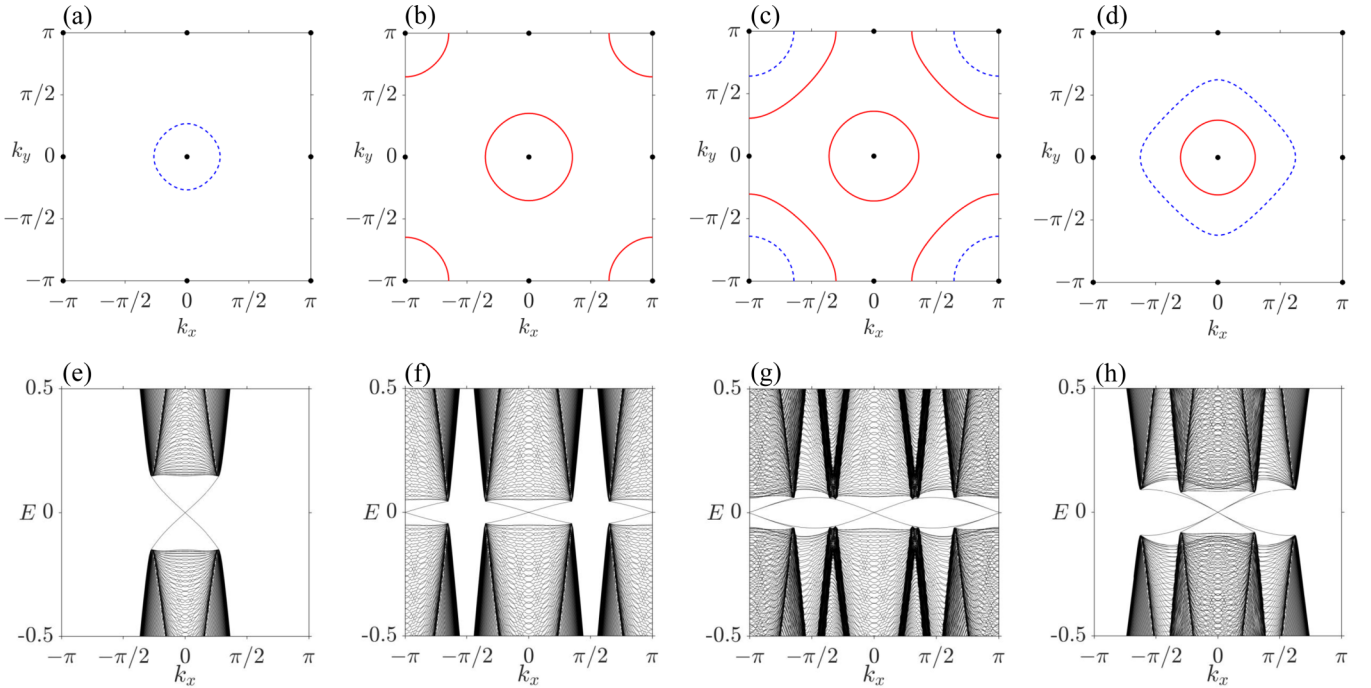


FIG. 5. Fermi surfaces of the normal state and the edge states of the corresponding odd-parity superconducting phases. From (a)–(d), $\{m, \mu\} = \{5, 1\}$, $\{0, 4\}$, $\{1, 3\}$, and $\{4, 2\}$, respectively. The black dots in (a)–(d) represent the locations of the four time-reversal invariant momenta in the two-dimensional Brillouin zone. The dashed blue/solid red lines refer to the Fermi surfaces contributed by the first/second pair of conduction Kramers bands. Other parameters are chosen as $\{t, t_z, \lambda, \eta_1, \eta_2, \Delta_3\} = \{2, 1, 1, 0.25, 0.25, 0.5\}$. For the chosen parameters, The mirror Chern numbers for (a)–(d) are $C_M = 1, 2, 1$, and 0 , respectively. (e)–(h) Energy spectra for a sample with periodic boundary conditions in the x direction and open boundary conditions in the y direction. The parameters in (e)–(h) are the same as in (a)–(d), respectively. In (e), the midgap crossing at $k_x = 0$ is of fourfold degeneracy. In (f), the midgap crossings at $k_x = 0$ and $k_x = \pi$ are both of fourfold degeneracy. In (g), the midgap crossing at $k_x = 0$ is of fourfold degeneracy, but the one at $k_x = \pi$ is of eightfold degeneracy. In (h), the midgap crossing at $k_x = 0$ is of eightfold degeneracy.

helical Majorana edge states can show up even when $C_{M,s} = 0$ as a consequence of the existence of additional symmetries on certain high symmetry lines in the Brillouin zone.

To demonstrate the bulk-boundary correspondence, we consider a sample of the geometry with periodic boundary conditions in the x direction and open boundary conditions in the y direction. Figures 5(a) and 5(e) show when there is only one piece of Fermi surface enclosing one time-reversal invariant momentum in the normal state, the superconductor harbors one pair of helical Majorana edge states, in agreement with the Z_2 invariant given by Eq. (14). The property of the edge states indicates that the superconductor is a time-reversal invariant first-order topological superconductor. In comparison, Figs. 5(b) and 5(f) show when there are two pieces of Fermi surfaces enclosing two distinct time-reversal invariant momenta, the superconductor harbors two pairs of helical Majorana edge states. By calculating the mirror Chern number contributed by all negative energy bands, we find $C_{M,s} = 2$, which is consistent with the number of pairs of helical Majorana edge states, indicating that the resulting superconductor is a topological mirror superconductor. These two cases show explicitly that if each piece of Fermi surfaces only encloses one time-reversal invariant momentum, the parity of the number of pairs of helical Majorana edge states is equal to the parity of the number of pieces of Fermi surfaces, i.e., Eq. (14). In Figs. 5(c), 5(d), 5(g), and 5(h) we further consider two cases for which there are two pieces of Fermi

surfaces enclosing the same time-reversal invariant momentum. In Figs. 5(c) and 5(g) the midgap crossing at $k_x = \pi$ is of eightfold degeneracy and the one at $k_x = 0$ is of fourfold degeneracy, suggesting the existence of three pairs of helical Majorana states on one edge. By calculating the mirror Chern number, however, we find $C_{M,s} = 1$, which is not equal to the number of helical Majorana edge modes. Similarly, Figs. 5(d) and 5(h) show the existence of two pairs of helical Majorana edge states, even though the mirror Chern number turns out to be zero. Here the discrepancy between the number of pairs of helical Majorana edge states and the mirror Chern number does not mean the breakdown of bulk-boundary correspondence. As we will explain below, the existence of additional pairs of helical Majorana edge states is a result of the existence of additional symmetries on high symmetry lines.

Let us take the result in Figs. 5(d) and 5(h) for illustration. The crossing at $k_x = 0$ is of eightfold degeneracy. If one views the BdG Hamiltonian $\mathcal{H}_{\text{BdG}}(k_x = 0, k_y)$ as a one-dimensional Hamiltonian, the eightfold degeneracy at $k_x = 0$ is equivalent to the existence of two Majorana Kramers pairs (four Majorana zero modes) per end in the one-dimensional system. However, the DIII class in one dimension also follows a Z_2 classification and can only support one robust Majorana Kramers pair per end [3–5]. According to the tenfold classification, only the three chiral symmetry classes follow a Z classification in one dimension and thus can support more than two zero-energy bound states per end. By analyzing the

symmetry of $\mathcal{H}_{\text{BDG}}(k_x = 0, k_y)$, we find that the Hamiltonian has an additional spinless time-reversal symmetry (the symmetry operator is $\mathcal{T} = \Sigma_{0030}\mathcal{K}$). Accordingly, $\mathcal{H}_{\text{BDG}}(k_x = 0, k_y)$ also belongs to the BDI class which permits multiple Majorana zero modes per end. Besides, as the Hamiltonian also has the mirror symmetry \mathcal{M}_x (the operator is $i\Sigma_{0010}$), on the high symmetry line $k_x = 0$, the Hamiltonian can also be decoupled into two independent parts according to the two eigenvalues of \mathcal{M}_x . We find that each mirror sector also belongs to the BDI class. By adding a term of the form $\gamma \sin k_y \Sigma_{3222}$ which preserves \mathcal{M}_z and the spinful time-reversal symmetry but breaks \mathcal{T} and \mathcal{M}_x , we find that the counterintuitive eightfold degeneracy is no longer protected, suggesting that the gapless nature of the edge states for the case with $C_{M,s} = 0$ is protected by these symmetries. The less robustness of the helical Majorana edge states for the case with $C_{M,s} = 0$ implies that such edge states are in principle gappable even without breaking the time-reversal symmetry and mirror symmetry \mathcal{M}_z . Once the Dirac masses hybridizing two pairs of helical Majorana edge states on two near-neighbor edges take opposite signs, the superconductor will evolve into a second-order topological superconductor with Majorana Kramers pairs at the corners of the system.

V. DISCUSSION AND CONCLUSION

We have shown that a bilayer Dirac system belonging to the D_{4h} symmetry group can support diverse topological insulating phases, including time-reversal invariant first-order topological insulators, topological mirror insulators, and second-order topological insulators. For topological mirror insulators, the mirror symmetry \mathcal{M}_z is essential. If the mirror symmetry is broken, for example, by substrate effects, an even number of pairs of helical edge states no longer have symmetry protection. Nevertheless, this does not mean that the topological mirror insulator will always transform to a trivial insulator after the lifting of mirror symmetry. In principle, it is also possible that the helical edge states hybridizes in a nontrivial way, leading to the emergence of higher-order topology. In experiments, these distinct types of topological insulating phases can be detected and distinguished by measuring the local density of states on the boundary [107,108] and the quantized conductance contributed by the helical edge states [109,110]. Taking advantage of the exceptional controllability of two-dimensional systems, topological phase transitions among them may also be accessible via methods such as strain and pressure.

When the bilayer system becomes metallic after doping, based on group-theoretical analysis and solving the linearized gap equations at the mean-field level, we found that the system favors odd-parity superconductivity when the short-range attractive interorbital interaction dominates over the intraorbital interaction. Depending on the number and positions of Fermi surfaces in the normal state, we find that the time-reversal invariant odd-parity superconductor can be a first-order topological superconductor, a topological mirror superconductor, or an exotic superconductor with an even number of pairs of helical edge states even though both the Z_2 invariant and the mirror Chern number are trivial.

In conclusion, our results show that bilayer Dirac materials can support diverse topological gapped phases both in the insulating state and in the superconducting state. Given the high controllability of two-dimensional materials and the experimental progress [111,112], our results reveal that bilayer Dirac materials could serve as a fertile playground for the study of topological phases and related topological phenomena.

ACKNOWLEDGMENTS

This work is supported by the National Natural Science Foundation of China (Grants No. 11904417 and No. 12174455) and the Natural Science Foundation of Guangdong Province (Grant No. 2021B1515020026). Hong-Hao Zhang is supported in part by the National Natural Science Foundation of China (NSFC) under Grant No. 11875327, the Fundamental Research Funds for the Central Universities, and the Sun Yat-Sen University Science Foundation.

APPENDIX A: LINEARIZED GAP EQUATIONS AND SUPERCONDUCTING SUSCEPTIBILITY

We begin with the Hamiltonian with on-site attractive interactions

$$H = \sum_{\mathbf{k}} \Psi^\dagger(\mathbf{k}) [\mathcal{H}_0(\mathbf{k}) - \mu] \Psi(\mathbf{k}) - U \sum_{i,\rho} (n_{i,1,\rho}^2 + n_{i,2,\rho}^2) - 2V \sum_{i,\rho} n_{i,1,\rho} n_{i,2,\rho}. \quad (\text{A1})$$

Here we have adopted a mixed description, with the free-particle Hamiltonian expressed in momentum space and the interactions expressed in real space. As introduced in the main text, U (V) refers to the strength of the intraorbital (interorbital) interaction and $n_{i,\sigma,\rho} = \sum_{s=\uparrow,\downarrow} c_{i,\sigma,s,\rho}^\dagger c_{i,\sigma,s,\rho}$ refers to the electron density operator for a given σ orbital at site i and layer ρ . In order to enter a superconducting phase, at least one of U and V is demanded to be positive.

At the mean-field level, the superconducting order parameter near the critical temperature is determined by the linearized gap equation [89,113]

$$\Delta_i = V_i \sum_j \chi_{ij} \Delta_j, \quad (\text{A2})$$

where the subscript i labels the representation of the superconducting order parameter in the given Nambu basis. For this model, $V_i = U$ or V , depending on whether Δ_i is induced by the intraorbital or interorbital interaction. The sum over j means a sum of all possible representations. The superconducting susceptibility is given by

$$\chi_{ij} = -\frac{1}{\beta} \sum_{\omega_n, \mathbf{k}} \text{Tr}[\Delta_i^\dagger G_e(\mathbf{k}, i\omega_n) \Delta_j G_h(\mathbf{k}, i\omega_n)], \quad (\text{A3})$$

where $\beta = 1/k_B T$ with k_B being the Boltzmann constant and T being the temperature, and the electron and hole Matsubara-Green functions are given by

$$G_e(\mathbf{k}, i\omega_n) = \{i\omega_n - [\mathcal{H}_0(\mathbf{k}) - \mu]\}^{-1}, \\ G_h(\mathbf{k}, i\omega_n) = \{i\omega_n + [\mathcal{H}_0(\mathbf{k}) - \mu]\}^{-1}. \quad (\text{A4})$$

The sum of the imaginary frequency in χ_{ij} is calculated by

$$\begin{aligned} \frac{1}{\beta} \sum_{i\omega_n, \mathbf{k}} F(i\omega_n, \mathbf{k}) &= \sum_{\mathbf{k}} \frac{-1}{2\pi i} \int_C f_D(z) F(z) dz \\ &= \sum_{\mathbf{k}} \frac{-1}{2\pi i} 2\pi i \sum_j \text{Res}[f_D(z_j) F(z_j)] \\ &= - \sum_{\mathbf{k}} \sum_j \text{Res}[f_D(z_j) F(z_j)], \end{aligned}$$

which will be used in the following calculations.

There are four distinct eigenvalues for $\mathcal{H}_0(\mathbf{k})$ at each \mathbf{k} . We label them as $\pm\epsilon_1(\mathbf{k})$ and $\pm\epsilon_2(\mathbf{k})$. Below for simplicity we focus on the limit with $\eta_1 = \eta_2 = 0$, accordingly $\epsilon_1(\mathbf{k}) = \sqrt{[M(\mathbf{k}) - t_z]^2 + \lambda^2(\sin^2 k_x + \sin^2 k_y)}$ and $\epsilon_2(\mathbf{k}) = \sqrt{[M(\mathbf{k}) + t_z]^2 + \lambda^2(\sin^2 k_x + \sin^2 k_y)}$, where $M(\mathbf{k}) = m - t \cos k_x - t \cos k_y$. Each of the eigenvalues is doubly degenerate.

APPENDIX B: SUPERCONDUCTING SUSCEPTIBILITIES FOR PAIRINGS IN THE A_{1g} REPRESENTATION

The two pairing order parameters belonging to the A_{1g} representation both originate from the intraorbital interaction, hence $V_i = U$. The linearized gap equations for $\Delta_1 = (\Delta_{1,1}, \Delta_{1,2})^T$ become

$$\begin{aligned} \Delta_{1,1} &= U \chi_{1,11} \Delta_{1,1} + U \chi_{1,12} \Delta_{1,2}, \\ \Delta_{1,2} &= U \chi_{1,21} \Delta_{1,1} + U \chi_{1,22} \Delta_{1,2}. \end{aligned} \quad (\text{B1})$$

Here the first subscript 1 of $\Delta_{1,i}$ means that the two kinds of pairings both belong to the A_{1g} representation, and the second subscript corresponds to the label of these two kinds of pairings. The above gap equations can be rewritten in a matrix form:

$$\Delta_1 = \begin{pmatrix} U \chi_{1,11} & U \chi_{1,12} \\ U \chi_{1,21} & U \chi_{1,22} \end{pmatrix} \Delta_1. \quad (\text{B2})$$

In the weak-coupling regime, it is known that only a small energy window near the Fermi surface takes part in the superconducting instability, so one can make the approximation $\epsilon_1 \approx \epsilon_2 \approx \mu$ if the Fermi level crosses both bands with energy $\epsilon_1(\mathbf{k})$ and $\epsilon_2(\mathbf{k})$. Here, without generality, we consider $\mu > 0$, assuming electron doping. The superconducting susceptibilities are given by

$$\begin{aligned} \chi_{1,11} &= -\frac{1}{\beta} \sum_{i\omega_n, \mathbf{k}} \text{Tr}[\Delta_{1,1}^\dagger G_e(\mathbf{k}, i\omega_n) \Delta_{1,1} G_h(\mathbf{k}, i\omega_n)] \\ &\approx \frac{1}{\beta} \sum_{\mathbf{k}} \frac{1}{\xi_1} \tanh \frac{\beta \xi_1}{2} + \frac{1}{\xi_2} \tanh \frac{\beta \xi_2}{2}, \\ \chi_{1,12} &= \chi_{1,21} \\ &= -\frac{1}{\beta} \sum_{i\omega_n, \mathbf{k}} \text{Tr}[\Delta_{1,1}^\dagger G_e(\mathbf{k}, i\omega_n) \Delta_{1,2} G_h(\mathbf{k}, i\omega_n)] \\ &\approx \frac{1}{\beta} \sum_{\mathbf{k}} \frac{\Lambda_1}{\xi_1} \tanh \frac{\beta \xi_1}{2} + \frac{\Lambda_2}{\xi_2} \tanh \frac{\beta \xi_2}{2}, \end{aligned}$$

$$\begin{aligned} \chi_{1,22} &= -\frac{1}{\beta} \sum_{i\omega_n, \mathbf{k}} \text{Tr}[\Delta_{1,2}^\dagger G_e(\mathbf{k}, i\omega_n) \Delta_{1,2} G_h(\mathbf{k}, i\omega_n)] \\ &\approx \frac{1}{\beta} \sum_{\mathbf{k}} \frac{\Lambda_1^2}{\xi_1} \tanh \frac{\beta \xi_1}{2} + \frac{\Lambda_2^2}{\xi_2} \tanh \frac{\beta \xi_2}{2}, \end{aligned} \quad (\text{B3})$$

where $\xi_1 = \epsilon_1(\mathbf{k}) - \mu$ and $\xi_2 = \epsilon_2(\mathbf{k}) - \mu$, $\Lambda_1 = [M(\mathbf{k}) - t_z]/\mu$, and $\Lambda_2 = [M(\mathbf{k}) + t_z]/\mu$.

APPENDIX C: SUPERCONDUCTING SUSCEPTIBILITY FOR THE PAIRING IN THE A_{1u} REPRESENTATION

The pairing in the A_{1u} representation originates from the interorbital interaction, so $V_i = V$ for this case and the linearized gap equation is given by

$$\Delta_2 = V \chi_2 \Delta_2, \quad (\text{C1})$$

where

$$\begin{aligned} \chi_2 &= -\frac{1}{\beta} \sum_{i\omega_n, \mathbf{k}} \text{Tr}[\Delta_2^\dagger G_e(\mathbf{k}, i\omega_n) \Delta_2 G_h(\mathbf{k}, i\omega_n)] \\ &\approx \sum_{\mathbf{k}} \frac{1 - \Lambda_1^2}{\xi_1} \tanh \frac{\beta \xi_1}{2} + \frac{1 - \Lambda_2^2}{\xi_2} \tanh \frac{\beta \xi_2}{2}. \end{aligned} \quad (\text{C2})$$

APPENDIX D: SUPERCONDUCTING SUSCEPTIBILITY FOR THE PAIRING IN THE A_{2u} REPRESENTATION

The pairing in the A_{2u} representation also originates from the interorbital interaction, hence $V_i = V$ for this case and the linearized gap equation is given by

$$\Delta_3 = V \chi_3 \Delta_3, \quad (\text{D1})$$

where

$$\begin{aligned} \chi_3 &= -\frac{1}{\beta} \sum_{i\omega_n, \mathbf{k}} \text{Tr}[\Delta_3^\dagger G_e(\mathbf{k}, i\omega_n) \Delta_3 G_h(\mathbf{k}, i\omega_n)] \\ &\approx \sum_{\mathbf{k}} \frac{1 - \Lambda_1^2}{\xi_1} \tanh \frac{\beta \xi_1}{2} + \frac{1 - \Lambda_2^2}{\xi_2} \tanh \frac{\beta \xi_2}{2}. \end{aligned} \quad (\text{D2})$$

The result reveals $\chi_2 = \chi_3$. This degeneracy is a result of the considered limit $\eta_1 = \eta_2 = 0$ and will be lifted once they are nonzero. By numerically calculating the ground-state energy under the same condition, we find that Δ_3 will result in a smaller ground-state energy in comparison with Δ_2 when η_1 and η_2 are both nonzero, indicating that Δ_3 will win over Δ_2 .

APPENDIX E: SUPERCONDUCTING SUSCEPTIBILITIES FOR PAIRINGS IN THE E_u REPRESENTATION

The two pairing order parameters belonging to the E_u representation both originate from the interorbital interaction, hence $V_i = V$. The linearized gap equations for $\Delta_4 = (\Delta_{4,1}, \Delta_{4,2})^T$ are

$$\Delta_4 = \begin{pmatrix} V \chi_{4,11} & V \chi_{4,12} \\ V \chi_{4,21} & V \chi_{4,22} \end{pmatrix} \Delta_4. \quad (\text{E1})$$

where

$$\chi_{4,11} = -\frac{1}{\beta} \sum_{i\omega_n, \mathbf{k}} \text{Tr}[\Delta_{4,1}^\dagger G_e(\mathbf{k}, i\omega_n) \Delta_{4,1} G_h(\mathbf{k}, i\omega_n)]$$

$$\begin{aligned}
&\approx \sum_{\mathbf{k}} \frac{\lambda^2 \sin^2 k_y}{\mu^2 \xi_1} \tanh \frac{\beta \xi_1}{2} + \frac{\lambda^2 \sin^2 k_y}{\mu^2 \xi_2} \tanh \frac{\beta \xi_2}{2} \\
&\approx \frac{\chi_3}{2}, \\
\chi_{4,22} &= -\frac{1}{\beta} \sum_{i\omega_n, \mathbf{k}} \text{Tr}[\Delta_{4,2}^\dagger G_e(\mathbf{k}, i\omega_n) \Delta_{4,2} G_h(\mathbf{k}, i\omega_n)] \\
&\approx \sum_{\mathbf{k}} \frac{\lambda^2 \sin^2 k_x}{\mu^2 \xi_1} \tanh \frac{\beta \xi_1}{2} + \frac{\lambda^2 \sin^2 k_x}{\mu^2 \xi_2} \tanh \frac{\beta \xi_2}{2} \\
&\approx \frac{\chi_3}{2}, \\
\chi_{4,12} &= -\frac{1}{\beta} \sum_{i\omega_n, \mathbf{k}} \text{Tr}[\Delta_{4,1}^\dagger G_e(\mathbf{k}, i\omega_n) \Delta_{4,2} G_h(\mathbf{k}, i\omega_n)] = 0, \\
\chi_{4,21} &= -\frac{1}{\beta} \sum_{i\omega_n, \mathbf{k}} \text{Tr}[\Delta_{4,2}^\dagger G_e(\mathbf{k}, i\omega_n) \Delta_{4,1} G_h(\mathbf{k}, i\omega_n)] = 0.
\end{aligned} \tag{E2}$$

Above, the relation $\chi_{4,11} = \chi_{4,22}$ can be inferred from the C_{4z} symmetry of the Hamiltonian. For the relation $\chi_{4,11} = \chi_{4,22} \approx \chi_3/2$, it can be inferred from the fact that near the Fermi surface, according to the energy spectrum, one has $1 - \Lambda_{1,2}^2 \approx \lambda^2(\sin^2 k_x + \sin^2 k_y)/\mu^2$. This relation indicates that the pairings in the E_u representation will not be favored.

APPENDIX F: PAIRING PHASE DIAGRAM

Here we consider a concrete case to show how to determine the pairing phase diagram. Without loss of generality, we consider that the band minimum of the energy spectrum is located at the time-reversal invariant momentum $(k_x, k_y) = (0, 0)$. To analytically estimate the superconducting susceptibilities, we expand the Hamiltonian to the second order in momentum. Accordingly, we have

$$\begin{aligned}
\epsilon_{1,2} &= \sqrt{[M(\mathbf{k}) \pm t_z]^2 + (\sin^2 k_x + \sin^2 k_y)\lambda^2} \\
&\approx \sqrt{(m - 2t + \frac{tk^2}{2} \pm t_z)^2 + \lambda^2 k^2},
\end{aligned} \tag{F1}$$

where $k^2 = k_x^2 + k_y^2$. Near the two Fermi surfaces, the energies satisfy $\epsilon_{1,2}^2 \approx \mu^2$, accordingly, we can solve k^2 on the Fermi surface. Therefore, the approximated $M(\mathbf{k})$ near the two Fermi surfaces are given by

$$\begin{aligned}
M_1 &= \frac{-\lambda^2 + \sqrt{2t\lambda^2(m - 2t - t_z) + \lambda^4 + t^2\mu^2}}{t} + t_z, \\
M_2 &= \frac{-\lambda^2 + \sqrt{2t\lambda^2(m - 2t + t_z) + \lambda^4 + t^2\mu^2}}{t} - t_z.
\end{aligned} \tag{F2}$$

Using the substitution $\sum_{\mathbf{k}} \rightarrow \int D(\xi_i) d\xi_i$, we obtain

$$\begin{aligned}
\chi_{1,11} &= \int d\xi_1 \frac{D(\xi_1)}{\xi_1} \tanh \frac{\beta \xi_1}{2} + \int d\xi_2 \frac{D(\xi_2)}{\xi_2} \tanh \frac{\beta \xi_2}{2}, \\
\chi_{1,12} &= \chi_{1,21} = \int d\xi_1 \frac{D(\xi_1)\Lambda_1}{\xi_1} \tanh \frac{\beta \xi_1}{2} \\
&\quad + \int d\xi_2 \frac{D(\xi_2)\Lambda_2}{\xi_2} \tanh \frac{\beta \xi_2}{2},
\end{aligned}$$

$$\begin{aligned}
\chi_{1,22} &= \int d\xi_1 D(\xi_1) \frac{\Lambda_1^2}{\xi_1} \tanh \frac{\beta \xi_1}{2} \\
&\quad + \int d\xi_2 D(\xi_2) \frac{\Lambda_2^2}{\xi_2} \tanh \frac{\beta \xi_2}{2}, \\
\chi_2 &= \chi_3 = \int d\xi_1 D(\xi_1) \frac{1 - \Lambda_1^2}{\xi_1} \tanh \frac{\beta \xi_1}{2} \\
&\quad + \int d\xi_2 D(\xi_2) \frac{1 - \Lambda_2^2}{\xi_2} \tanh \frac{\beta \xi_2}{2}, \\
\chi_{4,11} &= \chi_{4,22} = \frac{\chi_3}{2}, \\
\chi_{4,12} &= \chi_{4,21} = 0,
\end{aligned} \tag{F3}$$

where $\Lambda_1 = (M_1 - t_z)/\mu$ and $\Lambda_2 = (M_2 + t_z)/\mu$. The density of states is given by

$$\begin{aligned}
D(\xi_i) &= \int \frac{d^2k}{(2\pi)^2} \delta(\xi - \xi_i) \\
&= \int \frac{d\xi_i}{(2\pi)^2} \frac{(2\pi k) dk}{d\xi_i} \delta(\xi - \xi_i) \\
&= \frac{m_i^*}{2\pi},
\end{aligned} \tag{F4}$$

where we have used $\int d^2k = \int_0^{+\infty} k dk \int_0^{2\pi} d\theta = 2\pi \int_0^{+\infty} k dk$ and the approximation $\xi_i \approx \xi_0 + \frac{k^2}{2m_i^*}$. Series expansion of $\epsilon_{1,2}$ gives rise to

$$\begin{aligned}
m_1^* &= \frac{|m - 2t - t_z|}{(m - 2t - t_z)t + \lambda^2}, \\
m_2^* &= \frac{|m - 2t + t_z|}{(m - 2t + t_z)t + \lambda^2}.
\end{aligned} \tag{F5}$$

For the convenience of discussion, we introduce the following notations:

$$\begin{aligned}
D_1 &= D(\xi_1) = \frac{m_1^*}{2\pi}, \\
D_2 &= D(\xi_2) = \frac{m_2^*}{2\pi}.
\end{aligned} \tag{F6}$$

Only one independent equation is reserved for Δ_4 when considering Eq. (F3). Hence we simplify the notation $\chi_4 = \chi_{4,11} = \chi_{4,22}$, and all of the linearized gap equations become

$$\begin{aligned}
\det \left[\begin{pmatrix} U \chi_{1,11}(T_C^{\Delta_1}) & U \chi_{1,12}(T_C^{\Delta_1}) \\ U \chi_{1,21}(T_C^{\Delta_1}) & U \chi_{1,22}(T_C^{\Delta_1}) \end{pmatrix} - I_{2 \times 2} \right] &= 0, \\
V \chi_2(T_C^{\Delta_2}) &= 1, \\
V \chi_3(T_C^{\Delta_3}) &= 1, \\
V \chi_4(T_C^{\Delta_4}) &= 1,
\end{aligned} \tag{F7}$$

where

$$\begin{aligned}
\chi_{1,11} &= (D_1 + D_2)\chi_0, \\
\chi_{1,12} &= \chi_{1,21} = [D_1\Lambda_1 + D_2\Lambda_2]\chi_0, \\
\chi_{1,22} &= [D_1\Lambda_1^2 + D_2\Lambda_2^2]\chi_0, \\
\chi_2 &= \chi_3 = 2\chi_4 = [D_1(1 - \Lambda_1^2) + D_2(1 - \Lambda_2^2)]\chi_0,
\end{aligned} \tag{F8}$$

with $\chi_0 = \int d\xi \frac{1}{\xi} \tanh \frac{\beta\xi}{2}$ being the standard superconducting susceptibility normalized by density of states. With the upper and lower limits of the integration fixed, χ_0 is a monotonically increasing function of the inverse temperature β . By solving the equations in Eq. (F7), one can determine which pairing channel has the highest critical temperature. Apparently, since

$\chi_4 < \chi_2 = \chi_3$, the superconducting pairing Δ_4 always has a lower critical temperature than Δ_2 and Δ_3 , i.e., $T_C^{\Delta_4} < T_C^{\Delta_2} = T_C^{\Delta_3}$. On the other hand, we have mentioned previously that Δ_3 will win over Δ_2 when η_1 and η_2 are both nonzero, so the pairing phase boundary is determined by $\chi_1(T_C^{\Delta_1}) = \chi_3(T_C^{\Delta_3})$, which gives the typical form shown in Fig. 3.

- [1] M. Z. Hasan and C. L. Kane, Colloquium: Topological insulators, *Rev. Mod. Phys.* **82**, 3045 (2010).
- [2] X.-L. Qi and S.-C. Zhang, Topological insulators and superconductors, *Rev. Mod. Phys.* **83**, 1057 (2011).
- [3] A. P. Schnyder, S. Ryu, A. Furusaki, and A. W. W. Ludwig, Classification of topological insulators and superconductors in three spatial dimensions, *Phys. Rev. B* **78**, 195125 (2008).
- [4] A. Kitaev, Periodic table for topological insulators and superconductors, *AIP Conf. Proc.* **1134**, 22 (2009).
- [5] C.-K. Chiu, J. C. Y. Teo, A. P. Schnyder, and S. Ryu, Classification of topological quantum matter with symmetries, *Rev. Mod. Phys.* **88**, 035005 (2016).
- [6] L. Fu, Topological Crystalline Insulators, *Phys. Rev. Lett.* **106**, 106802 (2011).
- [7] Y. Ando and L. Fu, Topological crystalline insulators and topological superconductors: From concepts to materials, *Annu. Rev. Condens. Matter Phys.* **6**, 361 (2015).
- [8] C.-K. Chiu, H. Yao, and S. Ryu, Classification of topological insulators and superconductors in the presence of reflection symmetry, *Phys. Rev. B* **88**, 075142 (2013).
- [9] R.-J. Slager, A. Mesaros, V. Juričić, and J. Zaanen, The space group classification of topological band-insulators, *Nat. Phys.* **9**, 98 (2013).
- [10] T. Morimoto and A. Furusaki, Topological classification with additional symmetries from clifford algebras, *Phys. Rev. B* **88**, 125129 (2013).
- [11] K. Shiozaki and M. Sato, Topology of crystalline insulators and superconductors, *Phys. Rev. B* **90**, 165114 (2014).
- [12] C. Fang and L. Fu, New classes of three-dimensional topological crystalline insulators: Nonsymmorphic and magnetic, *Phys. Rev. B* **91**, 161105(R) (2015).
- [13] Z. Wang, A. Alexandradinata, R. J. Cava, and B. A. Bernevig, Hourglass fermions, *Nature (London)* **532**, 189 (2016).
- [14] J. Kruthoff, J. de Boer, J. van Wezel, C. L. Kane, and R.-J. Slager, Topological Classification of Crystalline Insulators through Band Structure Combinatorics, *Phys. Rev. X* **7**, 041069 (2017).
- [15] H. C. Po, A. Vishwanath, and H. Watanabe, Symmetry-based indicators of band topology in the 230 space groups, *Nat. Commun.* **8**, 50 (2017).
- [16] B. Bradlyn, L. Elcoro, J. Cano, M. G. Vergniory, Z. Wang, C. Felser, M. I. Aroyo, and B. A. Bernevig, Topological quantum chemistry, *Nature (London)* **547**, 298 (2017).
- [17] F. Zhang, C. L. Kane, and E. J. Mele, Surface State Magnetization and Chiral Edge States on Topological Insulators, *Phys. Rev. Lett.* **110**, 046404 (2013).
- [18] W. A. Benalcazar, B. A. Bernevig, and T. L. Hughes, Quantized electric multipole insulators, *Science* **357**, 61 (2017).
- [19] W. A. Benalcazar, B. A. Bernevig, and T. L. Hughes, Electric multipole moments, topological multipole moment pumping, and chiral hinge states in crystalline insulators, *Phys. Rev. B* **96**, 245115 (2017).
- [20] F. Schindler, A. M. Cook, M. G. Vergniory, Z. Wang, S. S. P. Parkin, B. A. Bernevig, and T. Neupert, Higher-order topological insulators, *Sci. Adv.* **4**, eaat0346 (2018).
- [21] Z. Song, Z. Fang, and C. Fang, $(d-2)$ -Dimensional Edge States of Rotation Symmetry Protected Topological States, *Phys. Rev. Lett.* **119**, 246402 (2017).
- [22] J. Langbehn, Y. Peng, L. Trifunovic, F. von Oppen, and P. W. Brouwer, Reflection-Symmetric Second-Order Topological Insulators and Superconductors, *Phys. Rev. Lett.* **119**, 246401 (2017).
- [23] Z. Yan, Higher-order topological insulators and superconductors, *Acta Phys. Sin.* **68**, 226101 (2019).
- [24] F. Schindler, Dirac equation perspective on higher-order topological insulators, *J. Appl. Phys.* **128**, 221102 (2020).
- [25] B. Xie, H.-X. Wang, X. Zhang, P. Zhan, J.-H. Jiang, M. Lu, and Y. Chen, Higher-order band topology, *Nat. Rev. Phys.* **3**, 520 (2021).
- [26] L. Fu and C. L. Kane, Superconducting Proximity Effect and Majorana Fermions at the Surface of a Topological Insulator, *Phys. Rev. Lett.* **100**, 096407 (2008).
- [27] L. A. Wray, S.-Y. Xu, Y. Xia, Y. S. Hor, D. Qian, A. V. Fedorov, H. Lin, A. Bansil, R. J. Cava, and M. Z. Hasan, Observation of topological order in a superconducting doped topological insulator, *Nat. Phys.* **6**, 855 (2010).
- [28] Y. S. Hor, A. J. Williams, J. G. Checkelsky, P. Roushan, J. Seo, Q. Xu, H. W. Zandbergen, A. Yazdani, N. P. Ong, and R. J. Cava, Superconductivity in $\text{Cu}_x\text{Bi}_2\text{Se}_3$ and Its Implications for Pairing in the Undoped Topological Insulator, *Phys. Rev. Lett.* **104**, 057001 (2010).
- [29] M. Kriener, K. Segawa, Z. Ren, S. Sasaki, and Y. Ando, Bulk Superconducting Phase with a Full Energy Gap in the Doped Topological Insulator $\text{Cu}_x\text{Bi}_2\text{Se}_3$, *Phys. Rev. Lett.* **106**, 127004 (2011).
- [30] L. Fu and E. Berg, Odd-Parity Topological Superconductors: Theory and Application to $\text{Cu}_x\text{Bi}_2\text{Se}_3$, *Phys. Rev. Lett.* **105**, 097001 (2010).
- [31] S. Sasaki, M. Kriener, K. Segawa, K. Yada, Y. Tanaka, M. Sato, and Y. Ando, Topological Superconductivity in $\text{Cu}_x\text{Bi}_2\text{Se}_3$, *Phys. Rev. Lett.* **107**, 217001 (2011).
- [32] S. Sasaki, Z. Ren, A. A. Taskin, K. Segawa, L. Fu, and Y. Ando, Odd-Parity Pairing and Topological Superconductivity in a Strongly Spin-Orbit Coupled Semiconductor, *Phys. Rev. Lett.* **109**, 217004 (2012).
- [33] T. H. Hsieh, H. Lin, J. Liu, W. Duan, A. Bansil, and L. Fu, Topological crystalline insulators in the SnTe material class, *Nat. Commun.* **3**, 982 (2012).
- [34] Y. Tanaka, Z. Ren, T. Sato, K. Nakayama, S. Souma, T. Takahashi, K. Segawa, and Y. Ando, Experimental realization

- of a topological crystalline insulator in SnTe, *Nat. Phys.* **8**, 800 (2012).
- [35] S.-Y. Xu, C. Liu, N. Alidoust, M. Neupane, D. Qian, I. Belopolski, J. D. Denlinger, Y. J. Wang, H. Lin, L. A. Wray, G. Landolt, B. Slomski, J. H. Dil, A. Marcinkova, E. Morosan, Q. Gibson, R. Sankar, F. C. Chou, R. J. Cava, A. Bansil *et al.*, Observation of a topological crystalline insulator phase and topological phase transition in $\text{Pb}_{1-x}\text{Sn}_x\text{Te}$, *Nat. Commun.* **3**, 1192 (2012).
- [36] T. Liang, Q. Gibson, J. Xiong, M. Hirschberger, S. P. Koduvayur, R. J. Cava, and N. P. Ong, Evidence for massive bulk Dirac fermions in $\text{Pb}_{1-x}\text{Sn}_x\text{Se}$ from Nernst and thermopower experiments, *Nat. Commun.* **4**, 2696 (2013).
- [37] Y. Okada, M. Serbyn, H. Lin, D. Walkup, W. Zhou, C. Dhital, M. Neupane, S. Xu, Y. J. Wang, R. Sankar, F. Chou, A. Bansil, M. Z. Hasan, S. D. Wilson, L. Fu, and V. Madhavan, Observation of Dirac node formation and mass acquisition in a topological crystalline insulator, *Science* **341**, 1496 (2013).
- [38] C. Yan, J. Liu, Y. Zang, J. Wang, Z. Wang, P. Wang, Z.-D. Zhang, L. Wang, X. Ma, S. Ji, K. He, L. Fu, W. Duan, Q.-K. Xue, and X. Chen, Experimental Observation of Dirac-like Surface States and Topological Phase Transition in $\text{Pb}_{1-x}\text{Sn}_x\text{Te}$ (111) Films, *Phys. Rev. Lett.* **112**, 186801 (2014).
- [39] C. M. Polley, P. Dziawa, A. Reszka, A. Szczerbakow, R. Minikayev, J. Z. Domagala, S. Szafer, P. Kacman, R. Buczko, J. Adell, M. H. Berntsen, B. M. Wojek, O. Tjernberg, B. J. Kowalski, T. Story, and T. Balasubramanian, Observation of topological crystalline insulator surface states on (111)-oriented $\text{Pb}_{1-x}\text{Sn}_x\text{Se}$ films, *Phys. Rev. B* **89**, 075317 (2014).
- [40] P. Zhang, K. Yaji, T. Hashimoto, Y. Ota, T. Kondo, K. Okazaki, Z. Wang, J. Wen, G. D. Gu, H. Ding *et al.*, Observation of topological superconductivity on the surface of an iron-based superconductor, *Science* **360**, 182 (2018).
- [41] D. Wang, L. Kong, P. Fan, H. Chen, S. Zhu, W. Liu, L. Cao, Y. Sun, S. Du, J. Schneeloch *et al.*, Evidence for Majorana bound states in an iron-based superconductor, *Science* **362**, 333 (2018).
- [42] Q. Liu, C. Chen, T. Zhang, R. Peng, Y.-J. Yan, C.-H.-P. Wen, X. Lou, Y.-L. Huang, J.-P. Tian, X.-L. Dong, G.-W. Wang, W.-C. Bao, Q.-H. Wang, Z.-P. Yin, Z.-X. Zhao, and D.-L. Feng, Robust and Clean Majorana Zero Mode in the Vortex Core of High-Temperature Superconductor $(\text{Li}_{0.84}\text{Fe}_{0.16})\text{OHFeSe}$, *Phys. Rev. X* **8**, 041056 (2018).
- [43] L. Kong, S. Zhu, M. Papaj, H. Chen, L. Cao, H. Isobe, Y. Xing, W. Liu, D. Wang, P. Fan, Y. Sun, S. Du, J. Schneeloch, R. Zhong, G. Gu, L. Fu, H.-J. Gao, and H. Ding, Half-integer level shift of vortex bound states in an iron-based superconductor, *Nat. Phys.* **15**, 1181 (2019).
- [44] P. Zhang, Z. Wang, X. Wu, K. Yaji, Y. Ishida, Y. Kohama, G. Dai, Y. Sun, C. Bareille, K. Kuroda *et al.*, Multiple topological states in iron-based superconductors, *Nat. Phys.* **15**, 41 (2019).
- [45] M. Kheirkhah, Z. Yan, and F. Marsiglio, Vortex-line topology in iron-based superconductors with and without second-order topology, *Phys. Rev. B* **103**, L140502 (2021).
- [46] R.-X. Zhang, W. S. Cole, and S. Das Sarma, Helical Hinge Majorana Modes in Iron-Based Superconductors, *Phys. Rev. Lett.* **122**, 187001 (2019).
- [47] X. Wu, W. A. Benalcazar, Y. Li, R. Thomale, C.-X. Liu, and J. Hu, Boundary-Obstructed Topological High- T_c Superconductivity in Iron Pnictides, *Phys. Rev. X* **10**, 041014 (2020).
- [48] M. Kheirkhah, Z.-Y. Zhuang, J. Maciejko, and Z. Yan, Surface Bogoliubov-Dirac cones and helical Majorana hinge modes in superconducting Dirac semimetals, *Phys. Rev. B* **105**, 014509 (2022).
- [49] S. Qin, C. Fang, F.-C. Zhang, and J. Hu, Topological Superconductivity in an Extended s -Wave Superconductor and Its Implication to Iron-Based Superconductors, *Phys. Rev. X* **12**, 011030 (2022).
- [50] S. Sasaki and T. Mizushima, Superconducting doped topological materials, *Physica C* **514**, 206 (2015).
- [51] K. S. Novoselov, A. K. Geim, S. V. Morozov, D. Jiang, Y. Zhang, S. V. Dubonos, I. V. Grigorieva, and A. A. Firsov, Electric field effect in atomically thin carbon films, *Science* **306**, 666 (2004).
- [52] J. Chen, H. J. Qin, F. Yang, J. Liu, T. Guan, F. M. Qu, G. H. Zhang, J. R. Shi, X. C. Xie, C. L. Yang, K. H. Wu, Y. Q. Li, and L. Lu, Gate-Voltage Control of Chemical Potential and Weak Antilocalization in Bi_2Se_3 , *Phys. Rev. Lett.* **105**, 176602 (2010).
- [53] S. Kezilebieke, M. N. Huda, V. Vaňo, M. Aapro, S. C. Ganguli, O. J. Silveira, S. Głodzik, A. S. Foster, T. Ojanen, and P. Liljeroth, Topological superconductivity in a van der Waals heterostructure, *Nature (London)* **588**, 424 (2020).
- [54] J. Alicea, New directions in the pursuit of Majorana fermions in solid state systems, *Rep. Prog. Phys.* **75**, 076501 (2012).
- [55] C. W. J. Beenakker, Search for Majorana fermions in superconductors, *Annu. Rev. Condens. Matter Phys.* **4**, 113 (2013).
- [56] S. R. Elliott and M. Franz, Colloquium: Majorana fermions in nuclear, particle, and solid-state physics, *Rev. Mod. Phys.* **87**, 137 (2015).
- [57] M. Sato and S. Fujimoto, Majorana fermions and topology in superconductors, *J. Phys. Soc. Jpn.* **85**, 072001 (2016).
- [58] X.-L. Qi, T. L. Hughes, S. Raghu, and S.-C. Zhang, Time-Reversal-Invariant Topological Superconductors and Superfluids in Two and Three Dimensions, *Phys. Rev. Lett.* **102**, 187001 (2009).
- [59] F. Zhang, C. L. Kane, and E. J. Mele, Time-Reversal-Invariant Topological Superconductivity and Majorana Kramers Pairs, *Phys. Rev. Lett.* **111**, 056402 (2013).
- [60] J. Wang, Y. Xu, and S.-C. Zhang, Two-dimensional time-reversal-invariant topological superconductivity in a doped quantum spin-Hall insulator, *Phys. Rev. B* **90**, 054503 (2014).
- [61] F. Yang, C.-C. Liu, Y.-Z. Zhang, Y. Yao, and D.-H. Lee, Time-reversal-invariant topological superconductivity in n -doped BiH, *Phys. Rev. B* **91**, 134514 (2015).
- [62] F. Parhizgar and A. M. Black-Schaffer, Highly tunable time-reversal-invariant topological superconductivity in topological insulator thin films, *Sci. Rep.* **7**, 9817 (2017).
- [63] A. Haim and Y. Oreg, Time-reversal-invariant topological superconductivity in one and two dimensions, *Phys. Rep.* **825**, 1 (2019).
- [64] R.-X. Zhang and S. Das Sarma, Intrinsic Time-Reversal-Invariant Topological Superconductivity in Thin Films of Iron-Based Superconductors, *Phys. Rev. Lett.* **126**, 137001 (2021).
- [65] Z. Yan, F. Song, and Z. Wang, Majorana Corner Modes in a High-Temperature Platform, *Phys. Rev. Lett.* **121**, 096803 (2018).

- [66] Q. Wang, C.-C. Liu, Y.-M. Lu, and F. Zhang, High-Temperature Majorana Corner States, *Phys. Rev. Lett.* **121**, 186801 (2018).
- [67] T. Liu, J. J. He, and F. Nori, Majorana corner states in a two-dimensional magnetic topological insulator on a high-temperature superconductor, *Phys. Rev. B* **98**, 245413 (2018).
- [68] T. Yoshida, M. Sigrist, and Y. Yanase, Topological Crystalline Superconductivity in Locally Noncentrosymmetric Multilayer Superconductors, *Phys. Rev. Lett.* **115**, 027001 (2015).
- [69] T. Yoshida, A. Daido, Y. Yanase, and N. Kawakami, Fate of Majorana Modes in CeCoIn₅/YbCoIn₅ Superlattices: A Test Bed for the Reduction of Topological Classification, *Phys. Rev. Lett.* **118**, 147001 (2017).
- [70] Y. Tsutsumi, M. Ishikawa, T. Kawakami, T. Mizushima, M. Sato, M. Ichioka, and K. Machida, UPT₃ as a topological crystalline superconductor, *J. Phys. Soc. Jpn.* **82**, 113707 (2013).
- [71] Y. Yanase and K. Shiozaki, Möbius topological superconductivity in UPT₃, *Phys. Rev. B* **95**, 224514 (2017).
- [72] Y. Ueno, A. Yamakage, Y. Tanaka, and M. Sato, Symmetry-Protected Majorana Fermions in Topological Crystalline Superconductors: Theory and Application to Sr₂RuO₄, *Phys. Rev. Lett.* **111**, 087002 (2013).
- [73] K. Nogaki, A. Daido, J. Ishizuka, and Y. Yanase, Topological crystalline superconductivity in locally noncentrosymmetric CeRh₂As₂, *Phys. Rev. Research* **3**, L032071 (2021).
- [74] A. Daido, T. Yoshida, and Y. Yanase, Z₄ Topological Superconductivity in UCoGe, *Phys. Rev. Lett.* **122**, 227001 (2019).
- [75] F. Zhang, J. Jung, G. A. Fiete, Q. Niu, and A. H. MacDonald, Spontaneous Quantum Hall States in Chirally Stacked Few-Layer Graphene Systems, *Phys. Rev. Lett.* **106**, 156801 (2011).
- [76] F. Wu, T. Lovorn, E. Tutuc, and A. H. MacDonald, Hubbard Model Physics in Transition Metal Dichalcogenide Moiré Bands, *Phys. Rev. Lett.* **121**, 026402 (2018).
- [77] F. Wu, T. Lovorn, E. Tutuc, I. Martin, and A. H. MacDonald, Topological Insulators in Twisted Transition Metal Dichalcogenide Homobilayers, *Phys. Rev. Lett.* **122**, 086402 (2019).
- [78] J. O. Island, X. Cui, C. Lewandowski, J. Y. Khoo, E. M. Spanton, H. Zhou, D. Rhodes, J. C. Hone, T. Taniguchi, K. Watanabe, L. S. Levitov, M. P. Zaletel, and A. F. Young, Spin-orbit-driven band inversion in bilayer graphene by the van der Waals proximity effect, *Nature (London)* **571**, 85 (2019).
- [79] J. M. Lu, O. Zheliuk, I. Leermakers, N. F. Q. Yuan, U. Zeitler, K. T. Law, and J. T. Ye, Evidence for two-dimensional Ising superconductivity in gated MoS₂, *Science* **350**, 1353 (2015).
- [80] Y. Saito, Y. Nakamura, M. S. Bahramy, Y. Kohama, J. Ye, Y. Kasahara, Y. Nakagawa, M. Onga, M. Tokunaga, T. Nojima, Y. Yanase, and Y. Iwasa, Superconductivity protected by spin-valley locking in ion-gated MoS₂, *Nat. Phys.* **12**, 144 (2016).
- [81] D. Costanzo, S. Jo, H. Berger, and A. F. Morpurgo, Gate-induced superconductivity in atomically thin MoS₂ crystals, *Nat. Nanotechnol.* **11**, 339 (2016).
- [82] X. Xi, Z. Wang, W. Zhao, J.-H. Park, K. T. Law, H. Berger, L. Forró, J. Shan, and K. F. Mak, Ising pairing in superconducting NbSe₂ atomic layers, *Nat. Phys.* **12**, 139 (2016).
- [83] E. Sajadi, T. Palomaki, Z. Fei, W. Zhao, P. Bement, C. Olsen, S. Luescher, X. Xu, J. A. Folk, and D. H. Cobden, Gate-induced superconductivity in a monolayer topological insulator, *Science* **362**, 922 (2018).
- [84] Y. Cao, V. Fatemi, S. Fang, K. Watanabe, T. Taniguchi, E. Kaxiras, and P. Jarillo-Herrero, Unconventional superconductivity in magic-angle graphene superlattices, *Nature (London)* **556**, 43 (2018).
- [85] Y. Cao, V. Fatemi, A. Demir, S. Fang, S. L. Tomarken, J. Y. Luo, J. D. Sanchez-Yamagishi, K. Watanabe, T. Taniguchi, E. Kaxiras, R. C. Ashoori, and P. Jarillo-Herrero, Correlated insulator behaviour at half-filling in magic-angle graphene superlattices, *Nature (London)* **556**, 80 (2018).
- [86] L. Balents, C. R. Dean, D. K. Efetov, and A. F. Young, Superconductivity and strong correlations in Moiré flat bands, *Nat. Phys.* **16**, 725 (2020).
- [87] E. Y. Andrei and A. H. MacDonald, Graphene bilayers with a twist, *Nat. Mater.* **19**, 1265 (2020).
- [88] C. N. Lau, M. W. Bockrath, K. F. Mak, and F. Zhang, Reproducibility in the fabrication and physics of Moiré materials, *Nature (London)* **602**, 41 (2022).
- [89] C.-X. Liu, Unconventional Superconductivity in Bilayer Transition Metal Dichalcogenides, *Phys. Rev. Lett.* **118**, 087001 (2017).
- [90] Y. Nakamura and Y. Yanase, Odd-parity superconductivity in bilayer transition metal dichalcogenides, *Phys. Rev. B* **96**, 054501 (2017).
- [91] S. Kanasugi and Y. Yanase, Multiple odd-parity superconducting phases in bilayer transition metal dichalcogenides, *Phys. Rev. B* **102**, 094507 (2020).
- [92] C. Xu and L. Balents, Topological Superconductivity in Twisted Multilayer Graphene, *Phys. Rev. Lett.* **121**, 087001 (2018).
- [93] C.-C. Liu, L.-D. Zhang, W.-Q. Chen, and F. Yang, Chiral Spin Density Wave and $d + id$ Superconductivity in the Magic-Angle-Twisted Bilayer Graphene, *Phys. Rev. Lett.* **121**, 217001 (2018).
- [94] D. M. Kennes, J. Lischner, and C. Karrasch, Strong correlations and $d + id$ superconductivity in twisted bilayer graphene, *Phys. Rev. B* **98**, 241407(R) (2018).
- [95] M. Fidrysiak, M. Zegrodnik, and J. Spałek, Unconventional topological superconductivity and phase diagram for an effective two-orbital model as applied to twisted bilayer graphene, *Phys. Rev. B* **98**, 085436 (2018).
- [96] Z.-Y. Zhuang and Z. Yan, Topological phase transitions and evolution of boundary states induced by Zeeman fields in second-order topological insulators, *Front. Phys.* **10**, 866347 (2022).
- [97] B. A. Bernevig, T. L. Hughes, and S.-C. Zhang, Quantum spin Hall effect and topological phase transition in HgTe quantum wells, *Science* **314**, 1757 (2006).
- [98] L. Fu and C. L. Kane, Topological insulators with inversion symmetry, *Phys. Rev. B* **76**, 045302 (2007).
- [99] J. C. Y. Teo, L. Fu, and C. L. Kane, Surface states and topological invariants in three-dimensional topological insulators: Application to Bi_{1-x}Sb_x, *Phys. Rev. B* **78**, 045426 (2008).
- [100] T. Rauch, M. Flieger, J. Henk, I. Mertig, and A. Ernst, Dual Topological Character of Chalcogenides: Theory for Bi₂Te₃, *Phys. Rev. Lett.* **112**, 016802 (2014).
- [101] M. Eschbach, M. Lanius, C. Niu, E. Młyńczak, P. Gospodarič, J. Kellner, P. Schüffelgen, M. Gehlmann, S. Döring, E. Neumann, M. Luysberg, G. Mussler, L. Plucinski, M.

- Morgenstern, D. Grützmacher, G. Bihlmayer, S. Blügel, and C. M. Schneider, Bi_1Te_1 is a dual topological insulator, *Nat. Commun.* **8**, 14976 (2017).
- [102] J. I. Facio, S. K. Das, Y. Zhang, K. Koepf, J. van den Brink, and I. C. Fulga, Dual topology in jacutingaite Pt_2HgSe_3 , *Phys. Rev. Materials* **3**, 074202 (2019).
- [103] N. Avraham, A. Kumar Nayak, A. Steinbok, A. Norris, H. Fu, Y. Sun, Y. Qi, L. Pan, A. Isaeva, A. Zeugner, C. Felser, B. Yan, and H. Beidenkopf, Visualizing coexisting surface states in the weak and crystalline topological insulator Bi_2TeI , *Nat. Mater.* **19**, 610 (2020).
- [104] X.-L. Qi, T. L. Hughes, and S.-C. Zhang, Topological invariants for the Fermi surface of a time-reversal-invariant superconductor, *Phys. Rev. B* **81**, 134508 (2010).
- [105] M. Sato, Topological properties of spin-triplet superconductors and Fermi surface topology in the normal state, *Phys. Rev. B* **79**, 214526 (2009).
- [106] F. Zhang, C. L. Kane, and E. J. Mele, Topological Mirror Superconductivity, *Phys. Rev. Lett.* **111**, 056403 (2013).
- [107] F. Schindler, Z. Wang, M. G. Vergniory, A. M. Cook, A. Murani, S. Sengupta, A. Y. Kasumov, R. Deblock, S. Jeon, I. Drozdov, H. Bouchiat, S. Guéron, A. Yazdani, B. A. Bernevig, and T. Neupert, Higher-order topology in bismuth, *Nat. Phys.* **14**, 918 (2018).
- [108] S. N. Kempkes, M. R. Slot, J. J. van den Broeke, P. Capiod, W. A. Benalcazar, D. Vanmaekelbergh, D. Bercioux, I. Swart, and C. Morais Smith, Robust zero-energy modes in an electronic higher-order topological insulator, *Nat. Mater.* **18**, 1292 (2019).
- [109] M. König, S. Wiedmann, C. Brüne, A. Roth, H. Buhmann, L. W. Molenkamp, X.-L. Qi, and S.-C. Zhang, Quantum spin Hall insulator state in HgTe quantum wells, *Science* **318**, 766 (2007).
- [110] S. Wu, V. Fatemi, Q. D. Gibson, K. Watanabe, T. Taniguchi, R. J. Cava, and P. Jarillo-Herrero, Observation of the quantum spin Hall effect up to 100 Kelvin in a monolayer crystal, *Science* **359**, 76 (2018).
- [111] M. Liao, Y. Zang, Z. Guan, H. Li, Y. Gong, K. Zhu, X.-P. Hu, D. Zhang, Y. Xu, Y.-Y. Wang, K. He, X.-C. Ma, S.-C. Zhang, and Q.-K. Xue, Superconductivity in few-layer stanene, *Nat. Phys.* **14**, 344 (2018).
- [112] A. Devarakonda, H. Inoue, S. Fang, C. Ozsoy-Keskinbora, T. Suzuki, M. Kriener, L. Fu, E. Kaxiras, D. C. Bell, and J. G. Checkelsky, Clean 2D superconductivity in a bulk van der Waals superlattice, *Science* **370**, 231 (2020).
- [113] W. Yang, C.-J. Mo, S.-B. Fu, Y. Yang, F.-W. Zheng, X.-H. Wang, Y.-A. Liu, N. Hao, and P. Zhang, Soft-Mode-Phonon-Mediated Unconventional Superconductivity in Monolayer $1\text{T}'\text{-WTe}_2$, *Phys. Rev. Lett.* **125**, 237006 (2020).